

Catalytic reduction of dinitrogen to silylamines by earth-abundant lanthanide and group 4 complexes

Anthony Wong,¹ Matthew Hernandez,¹ Jaden Lara,¹ Francis Y. T. Lam,¹ T. Michael Trinh,¹ Rory P. Kelly,¹ Tatsumi Ochiai,¹ Guodong Rao,² R. David Britt,² Nikolas Kaltsoyannis,³ and Polly L. Arnold*¹

1. University of California, Berkeley, and Lawrence Berkeley National Laboratory; Berkeley, California CA 94720, US.

2. University of California, Davis; Davis, California CA 95616, US.

3. Department of Chemistry, University of Manchester, Oxford Road, Manchester M13 9PL, UK.

*Corresponding author. Email: pla@berkeley.edu

Abstract:

Dinitrogen is a challenging molecule to activate and reduce to useful products such as ammonia. The range of d-block metal complexes that can catalyze dinitrogen reduction to ammonia or tris(silyl)amines under ambient conditions has increased in recent years, and now includes more electropositive metal complexes, rather than the traditional electron-rich middle and late d-block cations used by nature and industry. Conventional f-block metal complexes do not have filled d-orbitals that would enable binding of N₂. Here, arene-bridged tetraphenolates are used to form metallacyclic structures by coordination to lanthanide or group 4 cations that can bind dinitrogen in the cavity and catalyze its conversion to bis(silyl)amines in ambient conditions. The unusual double-substitution product is attributed to the steric control afforded by the metalacycle's pocket. This is the first time that lanthanide complexes (and zirconium) have been shown to catalyze nitrogen reduction, and the reactivity of the most active, samarium, is attributed to the strong, yet accessible, reducing capacity of its divalent oxidation state, and the ability of the structure to retain group 1 metal cations in the catalyst coordination sphere. The group 4 complexes featuring small cavities are most selective for the formation of bis(silyl)amine, while the lanthanide complexes, with larger cavities, are also able to make the traditional tris(silyl)amine product from N₂. A series of experimental, analytical, spectroscopic, and computational studies provide insight into the mechanism of the reductive functionalization. These results offer new catalytic applications for plentiful titanium and the more earth-abundant members of the lanthanide series that are also less toxic than many base metals used in catalysis, such as iron.

Introduction

One of the most interesting challenges in bond activation chemistry is dinitrogen (N_2). The strong $N\equiv N$ bond (BDFE = 945 kJ mol^{-1}) and large HOMO–LUMO gap (10.82 eV) result in a high activation energy barrier and significant energy input requirement for the nitrogen reduction reaction, N_2RR .¹ Taking inspiration from nature, electron-rich, mid- d-block complexes^{2–7} have been widely studied for the reductive functionalization of N_2 to ammonia or the protected equivalent tris(trimethylsilyl)amine $N(\text{SiMe}_3)_3$, Scheme 1a. The number of complexes showing turnover has recently started to increase rapidly. For example, one of the most successful studies to date has focused on developing a family of Mo-based PXP ($X = \text{C, N, P}$) pincer complexes that convert N_2 to NH_3 . Through extensive catalyst optimization involving tuning of both the ligand and the reaction conditions, yields have improved with each generation from 12 equiv. ammonia per Mo atom, to thousands, although the most effective catalysis is stoichiometric in Sm^{II} reductant.^{8–14}

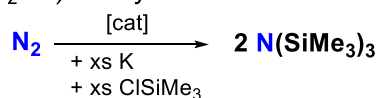
N_2RR catalysts with Lewis acidic early d-block metals are significantly rarer. A small number of titanium complexes have been reported to affect catalytic reductive functionalization of dinitrogen.¹⁵ In the 1990's Mori and coworkers reported that the reaction of $\text{Ti}(\text{O}^i\text{Pr})_4$ with lithium, 45 equiv. Me_3SiCl , and dinitrogen (1 atm) gave a mixture assumed to contain $[\text{ClTi}=\text{NSiMe}_3]$, $[\text{Cl}_2\text{Ti}-\text{N}(\text{SiMe}_3)_2]$, and $\text{N}(\text{SiMe}_3)_3$ which could subsequently be converted into benzamide by treatment with HCl .¹ The other previously reported homogeneous titanium N_2RR catalysts, both supported by the chelating, more electron-donating tren ligand, showed catalytic N_2RR forming up to 9 equiv. of NH_3 or 16.5 equiv. of $\text{N}(\text{SiMe}_3)_3$ per Ti .^{16–18}

N_2RR catalysts remain limited to d-block metals with the sole exception of our f-block metallacyclic uranium catalyst U_2L_2 ,¹⁹ where $\text{L} =$ the O-donor tetraphenolate $[\{2-(\text{OC}_6\text{H}_2-2\text{'Bu}, 4\text{'Me})_2\text{CH})-1,3\text{-C}_6\text{H}_4\}]^{20}$, which was able to catalyze the conversion of ambient N_2 to secondary silylamines in the presence of reductant, weak acid, and Me_3SiCl electrophile, generating 6.4 equivalents of amine per complex, Scheme 1b. Calculations, and the characterization of an intermediate containing the $[\text{N}_2\text{H}_2]^{2-}$ fragment suggested the reactive ligand C–H in L helps to deliver a proton to the activated N_2 ligand¹⁹ Prior to this, we had shown dinitrogen reduction by U^{III} centers with monodentate aryloxy or siloxide ligands, but reactions to target the further N_2 reduction needed for N-element bond formation resulted in O-ligand scrambling.^{21,22}

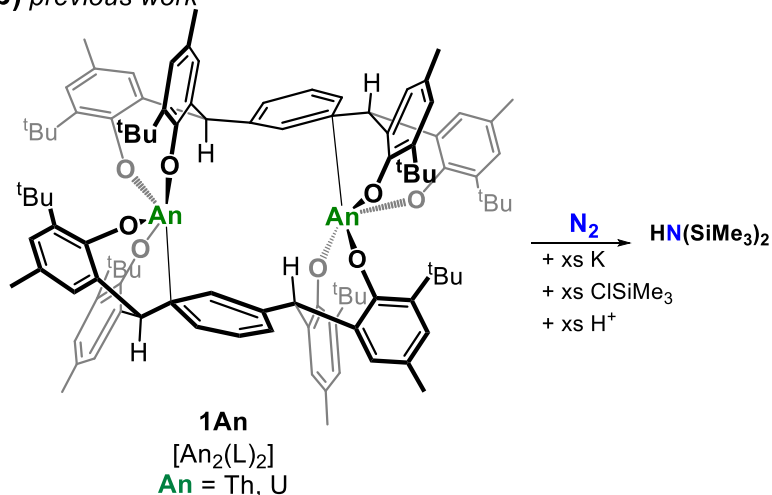
The U_2L_2 system was also the first time that a secondary amine had been formed by catalytic N_2RR using any catalyst.¹⁹ Our discovery of catalytic N_2RR by the uranium complex was unexpected since the valence electrons that electron rich d-block cations use to stabilize N_2 adducts, via back-bonding from metal to the unoccupied nitrogen π -orbitals, are not readily accessible to f-block metal cations, whose valence f-orbitals are contracted. The first evidence for N_2 binding in f-block chemistry came from the Sm^{II} organometallic complex Cp^*Sm , which exists in a dynamic equilibrium with the formally Sm^{III} dinitrogen adduct $\{\text{Cp}^*\text{Sm}\}_2(\mu\text{-N}_2)$ ($\text{Cp}^* = \eta\text{-C}_5\text{Me}_5$) in toluene solution under an N_2 atmosphere, demonstrating a minimally reduced N_2 group.²³ More recently, combining simple Ln^{III} complexes with K or KC_8 under a dinitrogen atmosphere forms complexes containing the N_2 dianion in the form $\{\text{X}_2\text{Ln}(\text{sol})_n\}_2(\mu\text{-N}_2)$ ($\text{Ln} = \text{Sc, Y, La} - \text{Nd, Gd} - \text{Tm, Lu}$; $\text{X} =$ bulky monodentate anionic O, N, or C-donor ligand, $\text{M} = \text{K}$, $n = 0\text{--}2$) and in some cases, triply reduced N_2 complexes $[\text{K}(\text{sol}')][\{\text{X}_2\text{Ln}(\text{sol})_n\}_2(\mu\text{-N}_2)]$ ($\text{Ln} = \text{Y, Er, and La, Gd} - \text{Er, Lu}$; $\text{sol} =$ monodentate– or crown–ether, or cryptand).^{24–31} This new family of complexes upturned ninety years of accepted wisdom by proving that rare earths can bind and reduce dinitrogen, helping the scientific community think differently about d- and f-orbital participation in bonding.^{32,33} Indeed, some of the complexes display remarkable magnetic properties as a result of their unusual electronic structures.³⁴ However, the only rare earth complexes that have shown N-element bond formation to date are the methylation of the N_2 trianion in $[\{\text{X}_2\text{Sc}\}_2(\mu\text{-N}_2)]^-$ which forms a $(\text{N}_2\text{Me}_2)^{2-}$ unit;³⁵ and protonation of the side-on, reduced N_2 - yttrium analogue with $[\text{HNEt}_3][\text{BPh}_4]$ which forms a crystallographically characterized bridging $(\text{N}_2\text{H}_2)^{2-}$ unit.³⁶

We considered the most important feature of our N_2RR catalysis to be the formation of secondary amine $\text{HN}(\text{SiMe}_3)_2$. Here we show that earth-abundant 4f and group 4 metal congeners of the U_2L_2 system can form metallacyclic catalysts for the conversion of N_2 to bis(silyl)amines at ambient conditions. The f-block complexes can also catalyze the transformation of N_2 to tris(silyl)amines highlighting the increased flexibility of f-block coordination complexes compared to the d-block.³⁷

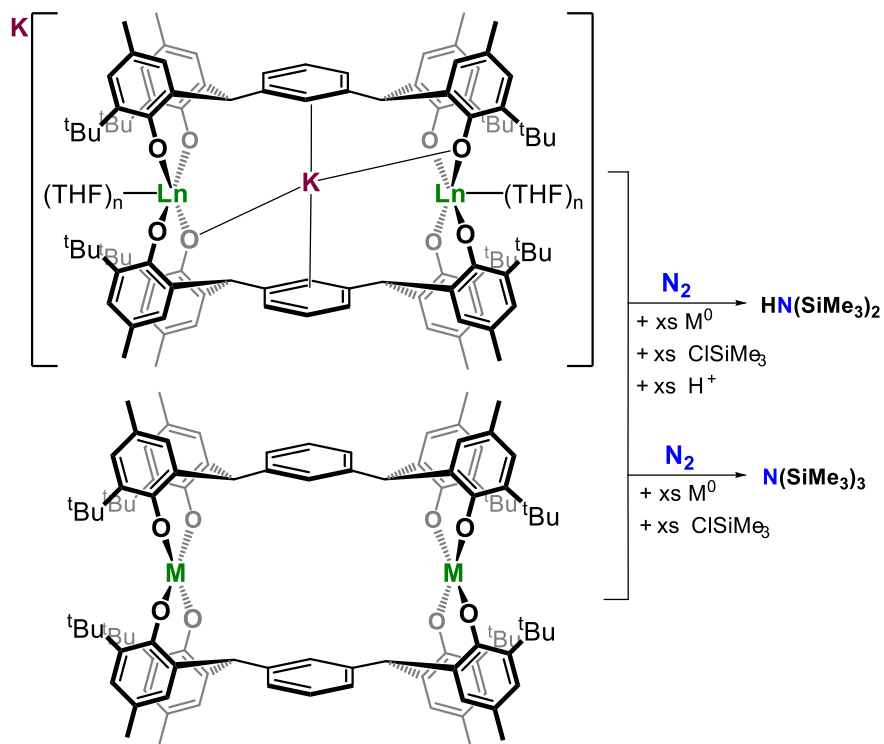
a) Nitrogen Reduction Reaction (N_2RR) to Silylamines



b) previous work



c) this work



Scheme 1 The N_2RR catalysts $1Ln$ and $1Ti/Zr$. (a) Generic catalyzed reaction for the conversion of N_2 to tris(silyl)amine. (b) Previous work on the tetravalent actinide complexes as catalysts for N_2RR and (c) this work on lanthanide and Group 4 complexes that catalyze the ambient conversion of N_2 to secondary amines. Ln = Sm, n = 3; Ce, n = 4; M = Ti, Zr; xs. = excess.

Results

The colorless bis-Ln^{III} metalacycle [K₂Ln₂(L)₂(THF)_n] **1Ln** (Ln = Ce, n=4, Sm, n=3), and M^{IV} metalacycle [M₂(L)₂] **1M**, M = Ti yellow, Zr colorless), are made from protonolysis reactions between the metal precursor and the tetraphenol H₄L in THF or arene solvent. The molecules, Scheme 1c, have been fully characterized, including by single crystal X-ray diffraction, see Figure S70–S76 and Figure 1. Complex **1Ti** is air stable.

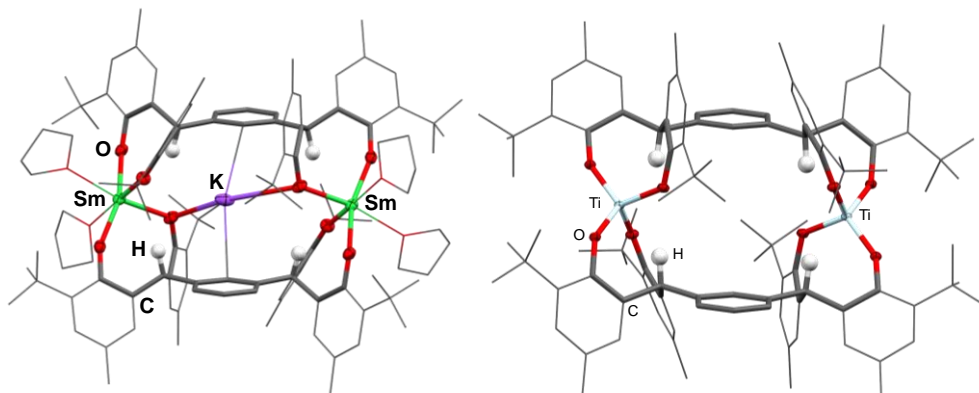


Figure 1 Structure of the N₂RR catalysts **1Sm** and **1Ti**. (a) **1Sm**.THF. (b) **1Ti**. Hydrogen atoms, lattice solvent and the [K(THF)₆] counter-cation for **1Sm** are omitted for clarity. The inter-lanthanide/group 4 metal cation distances are Sm1–Sm2 = 9.3830(7) Å, Ce1–Ce2 = 9.3706(5) Å, Ti1–Ti2 = 7.8902(4) Å and Zr1–Zr2 = 7.8241(7) Å (see SI).

The shape and potential for reactivity within the metalacycle pocket is of greatest interest. The solid-state structure of **1Sm** shows two octahedral Sm centers that form a rectangular cavity by coordinating two anionic aryloxy donors of each tetraanionic L, Figure 1a. In contrast, **1Ti** shows two tetrahedral Ti centers (Figure 1b).

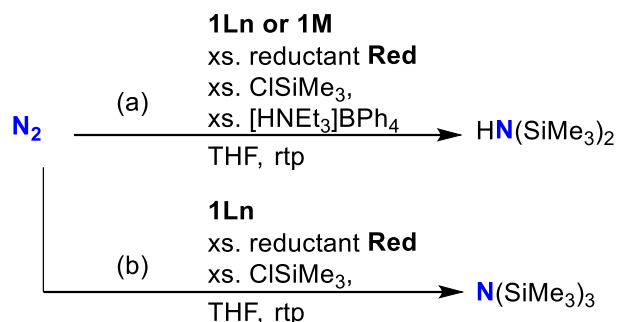
The Sm–Sm distance in **1Sm** is 9.3830(7) Å, significantly longer than the U–U distances in **1U** (6.5732(5) Å) and the hydrazido adduct [K₄U₂(μ-η²:η²-N₂H₂)(L⁻)₂] (4.6422(7) Å) which contains the four-electron reduced N₂H₂ anion.¹⁹ However it is close to the U–U distance in **1U-THF**, 9.3069(7) Å,¹⁹ since the two additional THF ligands on each metal displace the weak U–C close contacts formed with the *meta*-arene in **1U**. The Ti–Ti distance in **1Ti** is 7.8902(4) Å and the Zr–Zr distance in **1Zr** is 7.8240(9) Å (Figure S76).

In **1Ln** and **1M** (Ln = Ce, Sm; M = Ti, Zr) all four benzylic H point into the metallacyclic cavity whereas in **1U** and **1U-THF** only two (one on each L) point inwards; the benzylic CH (C7 and C30) are further from the center of the cavity in **1Sm** than in **1U** by an average of 1.31 Å. The distance between the closest benzylic C(H) and the midpoint between the two Sm in **1Sm** or two Ti in **1Ti**, is 3.72 Å in **1Sm**, 3.70 Å in **1Ti**. In the solid-state there is one potassium counter-cation located in the **1Ln** cavity, with bonds to two phenolate O atoms and an η¹ interaction with the central carbon in the bridging arene of each L; the arenes are co-planar but offset. The other K⁺ counter-cation is external and solvated by six THF molecules. The structure of the cerium congener **1Ce** is very similar (see Figure S73) except for slightly longer Ce–O bonds (ionic radii: Ce(III) = 1.191 Å, Sm(III) = 1.131 Å).

Cyclic voltammetry data for THF solutions of **1Sm**, **1Ti**, and **1Zr** with NBu₄PF₆ supporting electrolyte are shown in Figures S1–S3. The cyclic voltammogram of **1Ti** contains two reversible reductions at E_{1/2} = -1.91 V and -2.11 V vs. Fc/Fc⁺ assigned as metal-based events.³⁸ No reduction events for **1Sm** or **1Zr** were measurable within the electrochemical solvent window, i.e. as far as -3.2 V vs Fc and the calculated Ce^{III/II} reduction potential is -3.5 V vs Fc.^{39,40}

Catalytic N₂RR

The metalacyclic complexes **1Ln** and **1M** are catalysts for the conversion of N₂ to bis(silyl)amine HN(SiMe₃)₂; the general reaction involves stirring a THF solution of the catalyst with an excess of potassium metal to provide electrons, excess chlorotrimethylsilane Me₃SiCl (electrophile), and excess weak acid [HNEt₃][BPh₄], under an ambient N₂ atmosphere, Scheme 1 Scheme 2a. Reactions of **1Ln** and **1M** were also carried out in the absence of acid to target catalytic N₂RR to the conventional tris(silyl)amine, Scheme 2b. A range of control reactions, and reactions under different conditions and with alternative reagents and isotopomers are also described in the SI.



Scheme 2 N₂RR catalyzed by the lanthanide and group 4 complexes 1Ln and 1M (Ln = Ce, Sm; M = Ti, Zr). (a) ambient temperature and pressure formation of HN(SiMe₃)₂ from N₂ catalyzed by the lanthanide metallacycles **1Ln** or **1M**, using a group 1 metal reductant **Red**, trimethylchlorosilane and a weak acid; (b) the conventional product N(SiMe₃)₃ can be made by **1Ln** if acid is omitted. rtp = room temperature and pressure; xs. = excess.

The most informative reactions are outlined in *Table 1*. Nitrogen reduction products are identified and quantified by ²⁹Si NMR spectroscopy and gas chromatography (GC) (Figures S33–S43, Figures S7–S9) and yields are reported as an average of three runs. Brief comments are included in the final column.

Table 1 Catalytic conversion of N₂ to silylamines by metalacycles **1Ln** and **1M** under ambient conditions.

entry	pre-catalyst	reductant Red (300 equiv.) ^a	ClSiMe ₃ equiv.	[HNEt ₃][BPh ₄] equiv. ^b	HN(SiMe ₃) ₂ equiv. ^c	N(SiMe ₃) ₃ equiv.	comment
1	1Ce	K	225	131	1.84	0.26	1Ce is stoichiometric with K as reductant
2	1Sm	K	225	131	3.71 ± 0.44	0	K gives best conversion for 1Sm
3	1Ce	Rb	300	0	0	2.80 ± 0.62	Rb gives best conversion for 1Ce
4	1Sm	Rb	300	0	0	3.29 ± 0.45	1Sm /K is a better catalytic pair than 1Sm /Rb
5	1Ce	K	300	0	0	1.21	always under 75 % (stoichiometric) yield of tris(silyl)amine
6	1Sm	K	300	0	0	5.44 ± 0.50	1Ln can make bis- or tris(silyl)amine
7	1Ti	K	225	131	29.7 ± 0.71	5.35 ± 0.57	K gives best selectivity (85 % for bis(silyl)amine)
8	1Ti	K	300	0	0	1.44	1M are inactive for tris(silyl)amine
9	1Zr	K	225	131	5.46 ± 0.58	2.74 ± 0.84	1Zr is a poorer catalyst than 1Ti
10 ^d	1Ti	K	225 (4x)	131 (4x)	75.9	8.16	recycling 1Ti gives so far 84.1 equiv.

Footnotes: (a) **Red** = reductant; (b) catalysis results with other weak acids are in the SI; (c) yields quoted for all these complexes are per molecule rather than per Ln/M; average of 3 or more runs; (d) catalyst longevity test, with more reagent added to recycled, post-run catalyst and product yield reported for the four collected runs.

Under an atmosphere of N₂ at room temperature complex **1Sm** catalytically converts dinitrogen to the bis(silyl)amine HN(SiMe₃)₂, forming 3.71 ± 0.44 equiv. of amine per **1Sm** on average, and 6.37 equiv. of

amine on one occasion, *Table 1*, entry 2. This is the second instance of catalytic N₂ reduction providing a selective route to secondary amine product formation, following from our identification of the U₂L₂ catalyst.¹⁹ Under the same conditions, **1Ce** produces silylamines in close to stoichiometric quantities, *Table 1*, entry 1, affording an average total of 2.1 equivalents of bis(silyl)amine and tris(silyl)amine by-product (see below) per molecule of **1Ce**, but both **1Ln** are catalytically active when Rb is used as the reducing metal, *Table 1*, entries 3 and 4.

In the absence of weak acid, **1Sm** is an even better catalyst for the conversion of N₂ to tris(silyl)amine, making on average 5.44 ± 0.50 equivalents per **1Sm**, but yields for **1Ce** are substoichiometric, *Table 1*, entries 5 and 6, unless Rb is used as the reductant partner, *Table 1*, entry 3, yielding 2.80 ± 0.62 equiv. tris(silyl)amine. For **1Sm**, K is the most effective group 1 metal reductant (**Red**) (*Table 1* and *Table S1*, entries 1–18).

Compound **1Ti** gives the highest turnovers for N₂RR in these or other Ti systems; up to 31.4 equivalents HN(SiMe₃)₂ are formed, and 37.6 equiv. silylamines in total, *Table 1*, entry 7 and *Table S2*, entry 2. The two reported homogeneous titanium N₂RR catalysts gave up to 9 equiv. of NH₃ or 16.5 equiv. of N(SiMe₃)₃ per Ti.^{16–18} The Zr metallacycle **1Zr** is the first Zr-based N₂RR catalyst, but is poorer and less selective than **1Ti**, forming HN(SiMe₃)₂ (5.46 ± 0.58 equiv.) and N(SiMe₃)₃ (2.74 ± 0.84 equiv), *Table 1*, entry 9. Interestingly, **1M** is inactive as a catalyst for the formation of N(SiMe₃)₃, with substoichiometric conversions of N₂ for either Ti or Zr congener, *Table 1*, entry 8 and *Table S2*, entry 20. We suggest this is due to insufficient space in the metallacycle for product turnover. As for **1Sm**, **1Ti**, and **1Zr**, K is also the most effective group 1 metal reductant (*Table S2*, entries 1–24). In all cases studied, sodium as **Red** gives little or no turnover for N₂RR. Replacement of the reductant K with Na for **1** result in sub-stoichiometric yields of the silylamines (e.g. 0.42 equiv. HN(SiMe₃)₂; 0.43 equiv. N(SiMe₃)₃ for **1Sm**). In these reactions, significant amounts of hydrogen gas are observed, arising from the acid and reductant reacting in the absence of the catalyst. The replacement of [HNEt₃]⁺ salts with other weak acids including [HPCy₃][Cl] and phenol are also described in the SI (*Figure S28*, *Table S2*, entries 6, 8–10).

Catalyst longevity for **1Ti** was tested by adding further reagent to the post-run catalyst, which yields a combined 84.1 equiv. of amine for the four collected runs, *Table 1*, entry 10. The SI contains the individual run data.

In the catalytic reactions to form HN(SiMe₃)₂, N(SiMe₃)₃ is a by-product from a secondary reaction between the newly formed HN(SiMe₃)₂ with K metal to form KN(SiMe₃)₂, which reacts with ClSiMe₃. To demonstrate this, aliquots of an N₂RR catalysis using **1Ti** were removed during the reaction and analyzed by GC. The formation of HN(SiMe₃)₂ increases over the first 9 hours (*Figure S10*) then plateaus and starts to decrease as the N(SiMe₃)₃ by-product starts to form (*Figure S12*). We repeated the kinetic study using the standard conditions, except replacing [HNEt₃][BPh₄] with [DNEt₃][BPh₄], and observed a qualitative decrease in the overall rate of formation of H/DN(SiMe₃)₂, which suggests that N–H bond formation/cleavage is involved in the rate-determining step (*Figure S11*).

Raman spectra of **2Sm** contain an absorption at 1337 cm^{-1} which is shifted to a lower energy (1306 cm^{-1}) for $^{15}\text{N-2Sm}$, consistent with a doubly reduced N_2 with double bond character (Figures S54–S56). Raman spectroscopy of **2Ti** shows the presence of an NN single bond. The absorption at $\nu(^{15}\text{N}_2) = 796\text{ cm}^{-1}$ in the Raman spectrum of the mixture reduced under $^{15}\text{N}_2$, $^{15}\text{N-2Ti}$ shows a bathochromic shift compared to **2Ti** ($\nu(^{14}\text{N}_2) = 846\text{ cm}^{-1}$), (Figures S58–S60). The shift is larger than predicted by the reduced mass calculation for the two N isotopes, which would be consistent with the involvement of the adjacent heavy atoms in this stretching mode. No N-H bonds were identified in **2Sm** or **2Ti** by FTIR spectroscopy. Addition of weak acid to either $^{15}\text{N-2Sm}$ or $^{15}\text{N-2Ti}$ also generates a doublet in the ^1H NMR spectrum at 7.35 ppm ($^1J_{\text{NH}} = 71.3\text{ Hz}$) indicative of $^{15}\text{NH}_4\text{Cl}$, confirming that the amine N is derived from N_2 (Figure S24 and Figure S29).

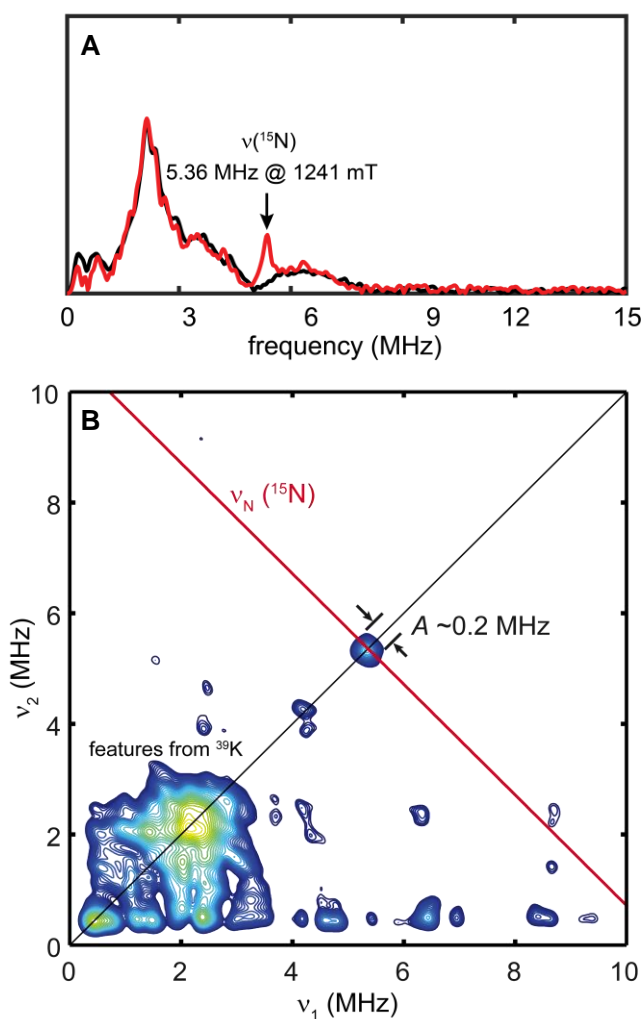


Figure 2 Q-band frequency domain 3-pulse ESEEM spectra (A) of $1\text{Ti-}^{14}\text{N}_2$ (black trace) and $1\text{Ti-}^{15}\text{N}_2$ (red trace) revealing a difference peak at 5.36 MHz, exactly at the Larmor frequency for ^{15}N at Q-band (1241 mT). Q-band HYSCORE spectrum (B) of $1\text{Ti-}^{15}\text{N}_2$ revealing the magnitude of the hyperfine coupling interaction of ^{15}N and Ti^{III} to be $\sim 0.2\text{ MHz}$. $T = 20\text{ K}$, $\pi/2 = 12\text{ ns}$, $\tau = 300\text{ ns}$.

For **2Ti**, we were able to remove the other paramagnetic Ti complexes, **K₂-1Ti** and **K₆-1Ti**, by fractional crystallization as they are particularly crystalline. We then used pulsed EPR spectroscopy to probe the N₂ binding in the remainder of **2Ti**, denoted **1Ti-N₂** and its isotopomer **1Ti-¹⁵N₂**. Q-band electron spin echo modulation (ESEEM) spectra are shown in Figure 2. Very interestingly, while the majority of the modulation patterns in the 3-pulse ESEEM spectra arise from coupling to ³⁹K, comparison between the frequency domain spectra of **1Ti-N₂** and **1Ti-¹⁵N₂** shows a sharp difference peak at 5.36 MHz, exactly at the Larmor frequency of ¹⁵N at Q-band (1241 mT). The coupling to ¹⁵N is corroborated by the two-dimensional hyperfine-sublevel correlation spectroscopy (HYSCORE), which clearly reveals a ¹⁵N coupling peak, with a very small hyperfine interaction of ~ 0.2 MHz, which likely arises from pure through-space electron nuclear dipole interactions; the magnitude of which implies very little, if any, orbital overlap between Ti^{III} and ¹⁵N. Assuming a small *T* of 0.1-0.2 MHz corresponds to Ti–N distance of 3-4 Å, which suggests that there are no direct covalent Ti–N bonds in **1Ti-N₂**.⁴¹ Given the Ti^{III}–Ti^{III} distance of 6.36 Å calculated from the spectra (see SI section 11) and estimated N–N bond length of 1.2-1.4 Å, the Ti–N distance suggested by EPR for **1Ti-N₂** is estimated as ~3.3 Å. Together, these data are consistent with a reduced N₂ unit positioned in the center of the ligand cavity oriented in a side-on fashion relative to the two Ti centers.

EPR spectra of frozen 2-Me-THF solutions of a number of independently synthesized samples of **2Sm** at 15 K show only a resonance assigned to an organic radical impurity and *g* = 2.005 without any discernable hyperfine features, Figure S66.

Discussion

Selectivity for secondary amine

This is the second instance of catalytic N₂ reduction providing a selective route to secondary amine product formation, following from our identification of the selective, but radioactive U₂L₂ catalyst. To the best of our knowledge, all other systems reported to date make tri-substituted amines in the presence of ClSiMe₃, except for Hidai's Mo(N₂)₂(PMe₂Ph)₄ complex, which catalytically converts N₂ into 8.1 equiv. of N-products with a HN(SiMe₃)₂:N(SiMe₃)₃ ratio of 13:83.⁴² The protons were suggested to derive from trace water. Sita devised a stoichiometric route to HN(SiMe₃)₂ by functionalizing a terminal Mo imido with sequential additions of acid and electrophile and reductant, as part of a synthetic cycle.⁴³

The **1Ln** precatalysts that can switch between making bis- and tris(silyl)amine have larger cavities and less rigid metal coordination geometries than **1Ti/Zr**, which cannot. While the **1Sm** and **1Ti** cavities are similarly narrow, it is reasonable to assume the six-coordinate, THF-coordinated Sm center has a greater degree of coordinative and structural flexibility than the tetrahedral Ti center. Further, the M-C_{benzylic} bonds in the dehydrometalated complexes make the cavity smaller and presumably more rigid, and the titanium adducts of L²⁻ are not active for N₂RR without the acid.

Identity of the Ln or group 4 metal, and cooperativity with the group 1 metal reductant

The Ln^{III} and M^{IV} metallacycles **1** all feature the stable metal oxidation state and strong Ln/M–O bonding that characterized the robust An^{IV} N₂RR catalysts. And as for the An^{IV} catalysts, there is no evidence of N₂ binding until **Red** is added. The long Ln/M distances in the cavity further support the importance of incorporating **Red** cations in the intermediates. In agreement, when we removed K cations from the coordination sphere of U₂(L)₂, no catalysis was observed.¹⁹ Mazzanti and Kawaguchi have noted the importance of group 1 counter-cation choice on stabilizing reduced N₂ complexes,^{44,45} while Holland has used different group 1 reductants, retained as counter-cations to control the number of iron complexes that can bind to and reduce N₂.⁴⁶

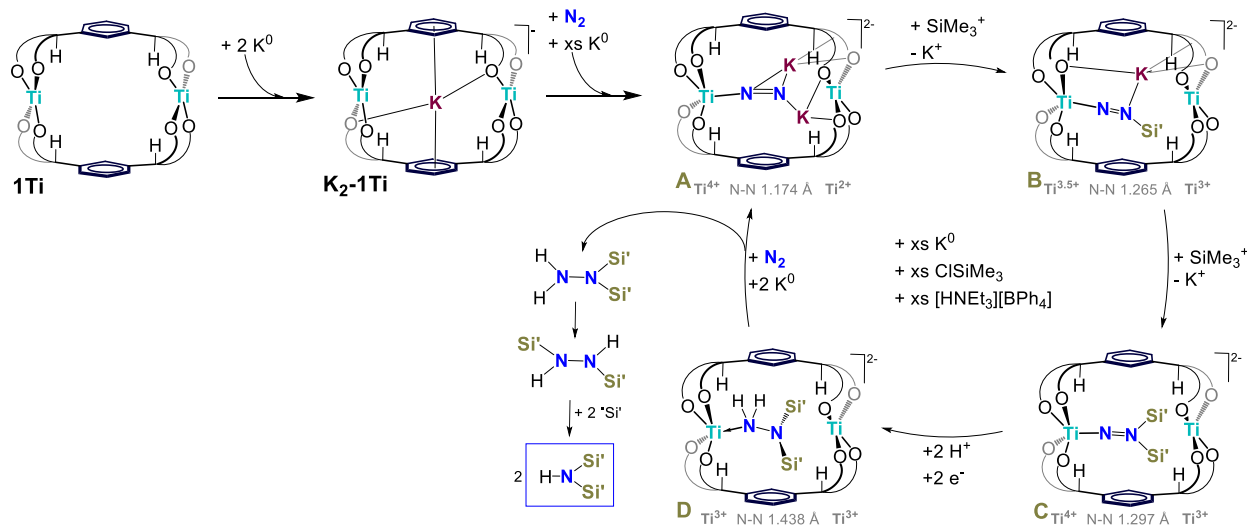
The better performances of the group 4 complexes than **1Ln** are probably due to kinetic factors. **1Ti** is air-stable, solid **1Zr** degrades slowly in air, and **1Ln** decomposes immediately upon exposure to air, and the reduced **2Ln** are exceptionally air-sensitive, making them more susceptible to side-reactions that terminate catalysis. However, the pairs can be compared: **1Sm** is a better catalyst than **1Ce**, and **1Ti** is better than **1Zr**; both **1Sm** and **1Ti** should be readily reduced by any **Red** in THF, suggesting these two metallacycles are better at providing an effective pathway for electrons to be delivered to the bound N₂ during the catalysis.⁴⁷ One reason for the greater reactivity of **1Sm** to make the tris(silyl)amine over the bis(silyl)amine is that the precatalyst shows some background reaction with the weak acid in the system.

The reaction of **1Sm** with [HNEt₃][BPh₄] (8 equiv.) in THF shows the release of some H₄L after one hour (Figure S48). Meanwhile, the group 4 complexes do not release H₄L, even after prolonged reaction times, which may be one reason why the bis(silyl)amine yields are higher than the **1Ln** pair.

Finally, the identity of the group 1 reductant **Red** is more important than the reduction potential. If the first reduction potential of the Lewis acidic metal Ln^{III/II} or M^{IV/III} in the metallocycle is less negative than the M^{0/I} potential of **Red** then catalytic N₂ reduction is better. The M^{0/I} potential for Na is -2.56 V and for K and Rb is -2.88 V vs Fc^{0/+} in MeCN.⁴⁸ We note that the reductive binding of N₂ at a Ln center with combinations of K metal and LnX₃ used by Evans et al work best for Ln^{III} that are relatively difficult to reduce, i.e. have reduction potentials that are close to that of the K^{+/0} redox couple. Although Group 4 metallocene complexes can bind and functionalize N₂,⁴⁹⁻⁵¹ catalytic functionalization was not reported, perhaps because the cyclopentadienyl ligands do not support a sufficiently reducing metal center.⁵² It is not clear why K is a better **Red** partner for **1Sm** but Rb is a better partner for **1Ce**, but could be due to a better size matching of the s-block cations that are stabilizing the reduced intermediates in the metallacyclic cavity. The inability of the smaller, harder sodium to function as an effective **Red** supports this.

Proposed mechanism

DFT calculations were undertaken to identify reaction intermediates for the catalytic cycle mediated by **1Ti** and the structures of catalytic intermediates are shown in *Scheme 3*.



Scheme 3 Structures of catalytic intermediates in the **1Ti** cycle, determined by DFT calculations. Si' = SiMe₃.

We begin with **1Ti**, modelled as a neutral singlet with two Ti(IV) centers. Calculation gives Ti–Ti = 7.813 Å and average Ti–O = 1.808 Å, which compare well with the experimental values of 7.890 Å and 1.812 Å respectively. From **1Ti** we move to **K₂-1Ti**, here modelled as a monoanionic triplet with only the internal K cation present, and the external counteranion excluded from the calculation. The structural agreement with experiment is once again very good: calculated Ti–Ti = 7.728 Å, Ti–K = 3.864 Å and average Ti–O = 1.913 Å, vs 7.676 Å, 3.838 Å and 1.914 Å from XRD. The Mulliken spin density is 1.029 on each Ti(III) center. At this stage we introduce an additional K, and an N₂ molecule. The latter was initially placed in a variety of starting orientations, midway between the two Ti centers and with overall C_i symmetry. Subsequent geometry optimizations of systems with different spin multiplicities yielded little evidence of N₂ reduction, with N–N distances close to that in free dinitrogen. Harmonic vibrational frequency analysis indicated that one of the converged geometries – a quintet in which the N₂ unit is oriented approximately along the Ti–Ti vector – is a transition state, with an imaginary mode of 69.2i cm⁻¹ corresponding to translation of the N₂ unit between the Ti centers. Removal of symmetry constraints, displacement along the imaginary mode,

and re-optimization of the geometry yielded a structure that is 67.3 kJ/mol more stable than the transition state, in which the N₂ unit bonds to only one of the Ti centers and the N–N distance lengthens to 1.172 Å.

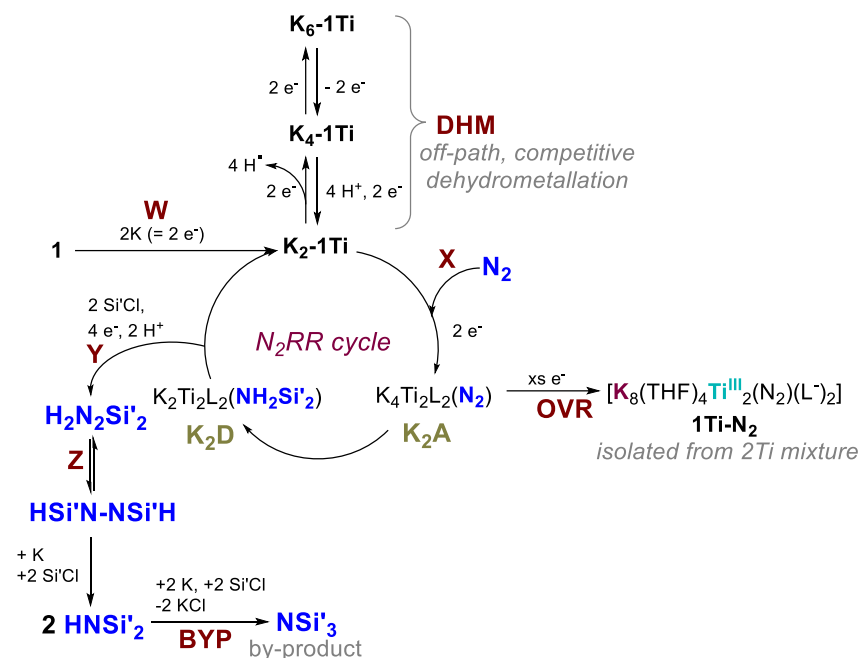
Subsequent re-optimisation of this system in different spin states established that the most stable structure is a triplet, 46.5 kJ/mol more stable than the quintet, and with a very similar geometry (N–N = 1.174 Å, Ti–N = 1.901 Å), intermediate **A** in Scheme 3. The spin density data suggest the N₂-bound Ti is Ti(IV), with minimal spin density on the N₂ unit. The other Ti center has spin density = 1.929. We were surprised to find that one Ti center plays the dominant role because almost all electropositive metal complexes containing reductively functionalized N₂ reported to date contain the reduced N₂ anion bound to two metals, and all these are symmetrical.²¹ However, we note that only **1Ti** and the two tren-supported complexes cited above^{16,17} have shown N₂RR catalysis. Moreover, the distal mechanism, which invokes end-on binding, is more common for those whose mechanism has been studied so far, and end-on bound N₂ is more reactive towards further functionalization than side-on N₂ in reported d-block chemistry.⁵³ Note also that, while the computed mechanism for N₂ reduction by our uranium-based catalyst¹⁹ featured side-onbound N₂ coordinated by both metals, the U–U distance in the precatalyst **1U** is ca. 1.3 Å shorter than the Ti–Ti distance in **1Ti** (which features significantly smaller metal ions). All reported Sm–N₂ complexes to date contain side-on bound N₂, yet a molecule of N₂ placed centrally in an end-on geometry in the cavity of the Sm^{III} starting material **1Sm** would have a Sm–N distance of 4.13 Å, too long for any significant orbital overlap. There is apparently minimal energy difference between the side-on and end-on bound (N₂)²⁻ adducts in the series {X₂Ln(sol)_n}₂(μ–N₂)^{24–32} complexes described above, although these are isolated for Ln^{III} that are hard to reduce, such as cerium. These data agree with the importance of the heterobimetallic combination of group 1 and Ln cations for the reactivity.

From **A** we move to species **B** in which one of the K ions bound to the distal N is replaced by SiMe₃⁺. This system, as with all the others in Scheme 3, except **1Ti** and **K₂-1Ti**, is a dianionic triplet. The spin density is distributed such that the N₂-free Ti is Ti(III), with the remainder spread over the other Ti (0.363) and the N₂ unit (0.538). The build-up of spin density on the latter is consistent with the lengthening of the N–N distance to 1.265 Å, in a formal [KSiMe₃N₂]^{–0.5} group. Replacement of the second N-bound K with SiMe₃⁺ leads to species **C**, in which there is greater spin density build-up on the N₂ (0.702) and an even longer N–N (1.297 Å). The N₂-free Ti remains Ti(III), and the Ti–N₂ distance remains short, 1.770 Å.

The final structure we have located is **D**. Two hydrogen atoms are added to the proximal N, leading to substantial changes in the spin density distribution and key distances. Both Ti centers are now Ti(III), and the N₂ unit now carries almost no net spin density. This is consistent with further lengthening of the N–N distance to 1.438 Å, an N–N single bond. The Ti–N₂ distance also lengthens substantially, and at 2.116 Å is now 0.346 Å longer than in **C**. The overall structure of **D** is essentially a doubly reduced version of **1Ti** with an H₂N₂(SiMe₃)₂ molecule sitting in the cavity, and the cavity limits silylation to two per N₂.

Release of the disilylhydrazine bound inside the Ti₂L₂ cavity, Scheme 3, is easy, and the 1,2 rearrangement of silylalkyl groups in disilylhydrazine is known to be rapid, so upon release from the cavity, H₂NNSi₂ rapidly forms the more stable 1,2-disilylhydrazine (**Z**),⁵⁴ that can react with the excess •SiMe₃ radicals^{55,56} to form the HN(SiMe₃)₂ product.

Roles of the precatalysts and off-cycle complexes in the proposed mechanism:



Scheme 4 Proposed catalytic N_2RR cycle for 1Ti (W, X) and the routes to amine release (Y, Z) and by-product formation (BYP), off-cycle competitive dehydrometalation (DHM), and over-reduction to $1\text{Ti}-\text{N}_2$ (OVR). The N_2 -containing intermediates $[\text{K}_2\text{Ti}_2\text{L}_2(\text{N}_2)]^{2-}$ K_2A and $[\text{Ti}_2\text{L}_2(\text{H}_2\text{NSi}'_2)]^{2-}$ K_2D , shown in Scheme 4, are expected to be on-cycle. e^- = electron derived from potassium metal; $\text{Si}' = \text{SiMe}_3$.

We combine the proposed mechanism for 1Ti with the off-cycle components for 1Ti in Scheme 4, recognizing that it is likely the same for 1Ln and 1Zr . From K_2-1Ti , two directions are possible: the N_2RR pathway, through X in which K_2-1Ti reacts with N_2 and K metal to form intermediate $[\text{K}_2\text{Ti}_2\text{L}_2(\text{N}_2)]^{2-}$, DFT structure K_2A in Scheme 3 or the competing off-cycle dehydrometalation pathway (DHM). The N_2RR pathway then follows through DFT structure D, drawn here as K_2D . The by-product $\text{N}(\text{SiMe}_3)_3$ can form from a secondary reaction (BYP) between $\text{HN}(\text{SiMe}_3)_2$ and reductant to yield $\text{KN}(\text{SiMe}_3)_2$ then an irreversible reaction with ClSiMe_3 .

The most highly reduced, metalated complexes such as N_2 -containing $1\text{Sm}-\text{N}_2$ and $1\text{Ti}-\text{N}_2$, and dehydrometalated K_4-1Ti and K_6-1Ti which are formed from overreduction prior to N_2 binding, and have the smallest cavities, are off-cycle. This is reasonable since it would be difficult to achieve this high level of reduction in the presence of acid and electrophile in the catalytic mixture. Nevertheless, 2Ln and 2Ti are active precatalysts, and K_4-1Ti and K_6-1Ti can both reform K_2-1Ti and re-enter the N_2RR cycle.

Conclusions

Metalacyclic group 4 and f-block complexes of tetradentate, bridging aryloxides are capable of binding dinitrogen in the cavity formed by the chelating aryloxide ligands upon reduction, even in a competing donor solvent such as THF. This enables the first non-radioactive instance of catalytic functionalization of dinitrogen to secondary amines; a product yet to be made catalytically by all the other d-block catalysts to date. The group 4 complexes selectively make the secondary amine in yields of up to 84.1 equivalents per complex, while the more coordinatively flexible f-block complexes can catalyze the N_2RR reaction to make either $\text{HN}(\text{SiMe}_3)_2$ or $\text{N}(\text{SiMe}_3)_3$ amine from ambient, atmospheric dinitrogen in yields of up to 6.4 and 7.8 equivalents per complex, respectively.

Kinetics and computational studies show that the bis(silyl)amine is the favored product and show how the ligand framework can help control the product selectivity by accommodating the additional group 1 counteranions associated with the reduction, such that the various reduced N_2 -containing intermediates

are stabilized. DFT calculations find end-on binding to just one of the metal centers, with the reducing group 1 metal cations stabilizing the other N prior to functionalization.

The N₂RR catalysis by **1Zr** is the first example for a zirconium complex to our knowledge. Comparing the pairs of catalysts **1Sm** vs. **1Ce** and **1Ti** vs. **1Zr** implies the accessibility of a one-electron reduced **M** that is, in turn, sufficiently reducing to a bound N₂, is most important here for N₂ reduction. Meanwhile, the size of the metalacyclic pocket is crucial in dictating the selectivity toward secondary amines for the smaller Group IV systems and to secondary or tertiary amines by the larger Ln. The differences between Na, K, and Rb as electron sources for N₂RR contribute additional datapoints to the growing body of as yet, unexplained importance of the choice of group 1 metal in heterobimetallic dinitrogen reduction chemistry.

In addition to demonstrating N₂RR catalysis with the most abundant of the lanthanides, the formation of secondary amines using plentiful titanium under ambient conditions is notable. The ability to function in polar solvents suggests the chemical reductant in these reactions could be replaced by a greener electrochemical source of electrons in the future.^{57,58}

Acknowledgments: The synthetic work was supported by the National Science Foundation (NSF, CHE-2154369) (ARW, PLA) and the U.S. Department of Energy (DOE), Office of Science, Office of Basic Energy Sciences, Chemical Sciences, Geosciences, and Biosciences Division, in the Catalysis Program and the Rare Earth Project in the Separations Program at the Lawrence Berkeley National Laboratory (FL, JKL, MH, ARW, MTT, PLA). The Catalysis Laboratory in the DOE Catalysis Program also provided resource and instrumentation used in this work and X-ray spectroscopic and some diffraction data were collected at Beamlines 8.0 and 12.2.1 of the Advanced Light Source, which is a DOE Office of Science User Facility. All of these DOE programs and facilities operate under contract no. DE-AC02-05CH11231. EPR spectroscopic studies were funded by the National Institutes of Health (NIH R35 grant 1R35GM126961 to RDB). Raman spectra were acquired using instrumentation provided by the Liquid Sunlight Alliance, which is supported by the US Department of Energy, Office of Science, Office of Basic Energy Sciences, Fuels from Sunlight Hub under award no. DE-SC0021266. Funding for CheXray comes from an NIH Shared Instrument Grant (S10-RR027172). We thank Hasan Celik for NMR spectroscopic support and discussions and the National Institutes of Health (NIH) for funding the UC Berkeley College of Chemistry NMR facility under grant no 1S10RR016634-01. We thank The University of Manchester for its Computational Shared Facility (CSF3, CSF4) and associated support services. We also thank the UK EPSRC for financial support through grant number EP/X042049/1. This project has also received funding for some of the early synthetic work from the European Research Council (ERC) under the European Union's Horizon 2020 research and innovation programme (grant agreement No 740311, PLA and RPK).

Authors Contributions: FYTL, ARW, MH, JKL, MTT, RPK, and TO made and characterized the compounds and reactions, and with PLA, analyzed the data and wrote the manuscript. GR and RDB collected and interpreted the EPR spectra. NK carried out and analyzed the mechanistic calculations, and wrote the DFT part of the manuscript. PLA raised the funding, conceptualized the project with contributions from FYTL, ARW, RDB, and NK, and all authors reviewed and edited the manuscript.

Declaration of Interests: An international patent application has been filed with the US receiving office, PCT/US23/74839.

Data availability: Crystallographic data in cif format are deposited at <https://ccdc.cam.ac.uk/>, codes 2181896-2181898, 2195247 and 2204194, 2210077 – 2210079, 2210081 – 2210083, 2307225.

Supplementary Information: Full synthetic and characterization data for the compounds and catalyses described. Computational details and xyz coordinates of the computed intermediates in Scheme 3.

Keywords: catalysis • dinitrogen reduction • N₂RR • EPR • DFT • lanthanides • actinides • titanium • zirconium • aryloxide

Supporting information: can be accessed online.

References and Notes:

1. Kuriyama, S., and Nishibayashi, Y. (2021). Development of catalytic nitrogen fixation using transition metal complexes not relevant to nitrogenases. *Tetrahedron* *83*, 131986. <https://doi.org/10.1016/j.tet.2021.131986>.
2. Yandulov, D.V., and Schrock, R.R. (2003). Catalytic reduction of dinitrogen to ammonia at a single molybdenum center. *Science* *301*, 76-78. 10.1126/science.1085326.
3. Sekiguchi, Y., Arashiba, K., Tanaka, H., Eizawa, A., Nakajima, K., Yoshizawa, K., and Nishibayashi, Y. (2018). Catalytic Reduction of Molecular Dinitrogen to Ammonia and Hydrazine Using Vanadium Complexes. *Angew. Chem. Int. Ed.* *57*, 9064-9068. <https://doi.org/10.1002/anie.201802310>.
4. Yin, J., Li, J., Wang, G.-X., Yin, Z.-B., Zhang, W.-X., and Xi, Z. (2019). Dinitrogen Functionalization Affording Chromium Hydrazido Complex. *J. Am. Chem. Soc.* *141*, 4241-4247. 10.1021/jacs.9b00822.
5. Anderson, J.S., Rittle, J., and Peters, J.C. (2013). Catalytic conversion of nitrogen to ammonia by an iron model complex. *Nature* *501*, 84. 10.1038/nature12435.
6. Piascik, A.D., Li, R., Wilkinson, H.J., Green, J.C., and Ashley, A.E. (2018). Fe-Catalyzed Conversion of N₂ to N(SiMe₃)₃ via an Fe-Hydrazido Resting State. *J. Am. Chem. Soc.* *140*, 10691-10694. 10.1021/jacs.8b06999.
7. Fajardo, J., Jr., and Peters, J.C. (2017). Catalytic Nitrogen-to-Ammonia Conversion by Osmium and Ruthenium Complexes. *J. Am. Chem. Soc.* *139*, 16105-16108. 10.1021/jacs.7b10204.
8. Ashida, Y., Mizushima, T., Arashiba, K., Egi, A., Tanaka, H., Yoshizawa, K., and Nishibayashi, Y. (2023). Catalytic production of ammonia from dinitrogen employing molybdenum complexes bearing N-heterocyclic carbene-based PCP-type pincer ligands. *Nature Synth.* *2*, 635-644. 10.1038/s44160-023-00292-9.
9. Arashiba, K., Miyake, Y., and Nishibayashi, Y. (2011). A molybdenum complex bearing PNP-type pincer ligands leads to the catalytic reduction of dinitrogen into ammonia. *Nature Chem.* *3*, 120-125. 10.1038/nchem.906.
10. Tanaka, H., Arashiba, K., Kuriyama, S., Sasada, A., Nakajima, K., Yoshizawa, K., and Nishibayashi, Y. (2014). Unique behaviour of dinitrogen-bridged dimolybdenum complexes bearing pincer ligand towards catalytic formation of ammonia. *Nature Communications* *5*, 3737. 10.1038/ncomms4737.
11. Arashiba, K., Kinoshita, E., Kuriyama, S., Eizawa, A., Nakajima, K., Tanaka, H., Yoshizawa, K., and Nishibayashi, Y. (2015). Catalytic Reduction of Dinitrogen to Ammonia by Use of Molybdenum–Nitride Complexes Bearing a Tridentate Triphosphine as Catalysts. *J. Am. Chem. Soc.* *137*, 5666-5669. 10.1021/jacs.5b02579.
12. Eizawa, A., Arashiba, K., Tanaka, H., Kuriyama, S., Matsuo, Y., Nakajima, K., Yoshizawa, K., and Nishibayashi, Y. (2017). Remarkable catalytic activity of dinitrogen-bridged dimolybdenum complexes bearing NHC-based PCP-pincer ligands toward nitrogen fixation. *Nature Commun.* *8*, 14874. 10.1038/ncomms14874.
13. Ashida, Y., Arashiba, K., Nakajima, K., and Nishibayashi, Y. (2019). Molybdenum-catalysed ammonia production with samarium diiodide and alcohols or water. *Nature* *568*, 536-540. 10.1038/s41586-019-1134-2.
14. Bora, D., Gayen, F.R., and Saha, B. (2022). Ammonia from dinitrogen at ambient conditions by organometallic catalysts. *RSC Adv.* *12*, 33567-33583. 10.1039/D2RA06156B.
15. Huang, W., Peng, L.-Y., Zhang, J., Liu, C., Song, G., Su, J.-H., Fang, W.-H., Cui, G., and Hu, S. (2023). Vanadium-Catalyzed Dinitrogen Reduction to Ammonia via a [V]=NNH₂ Intermediate. *J. Am. Chem. Soc.* 10.1021/jacs.2c08000.

16. Doyle, L.R., Wooles, A.J., Jenkins, L.C., Tuna, F., McInnes, E.J.L., and Liddle, S.T. (2018). Catalytic Dinitrogen Reduction to Ammonia at a Triamidoamine–Titanium Complex. *Angew. Chem. Int. Ed.* *57*, 6314–6318. 10.1002/anie.201802576.
17. Ghana, P., van Krüchten, F.D., Spaniol, T.P., van Leusen, J., Kögerler, P., and Okuda, J. (2019). Conversion of dinitrogen to tris(trimethylsilyl)amine catalyzed by titanium triamido-amine complexes. *Chem. Commun.* *55*, 3231–3234. 10.1039/C8CC09742A.
18. Sekiguchi, Y., Meng, F., Tanaka, H., Eizawa, A., Arashiba, K., Nakajima, K., Yoshizawa, K., and Nishibayashi, Y. (2018). Synthesis and reactivity of titanium- and zirconium-dinitrogen complexes bearing anionic pyrrole-based PNP-type pincer ligands. *Dalton Trans.* *47*, 11322–11326. 10.1039/C8DT02739K.
19. Arnold, P.L., Ochiai, T., Lam, F.Y.T., Kelly, R.P., Seymour, M.L., and Maron, L. (2020). Metallacyclic actinide catalysts for dinitrogen conversion to ammonia and secondary amines. *Nature Chem.* *12*, 654–659. 10.1038/s41557-020-0457-9.
20. Wells, J.A.L., Seymour, M.L., Suvova, M., and Arnold, P.L. (2016). Dinuclear uranium complexation and manipulation using robust tetraaryloxides. *Dalton Trans.* *45*, 16026–16032. 10.1039/C6DT02630C.
21. Mansell, S.M., Kaltsoyannis, N., and Arnold, P.L. (2011). Small molecule activation by uranium tris(aryloxides): Experimental and computational studies of binding of N₂, coupling of CO, and deoxygenation insertion of CO₂ under ambient conditions. *J. Am. Chem. Soc.* *133*, 9036–9051. 10.1021/ja2019492.
22. Mansell, S.M., Farnaby, J.H., Germeroth, A.I., and Arnold, P.L. (2013). Thermally stable uranium dinitrogen complex with siloxide supporting ligands *Organometallics* *32*, 4214. 10.1021/om4003957.
23. Evans, W.J., Ulibarri, T.A., and Ziller, J.W. (1988). Isolation and x-ray crystal structure of the first dinitrogen complex of an f-element metal, [(C₅Me₅)₂Sm]₂N₂. *J. Am. Chem. Soc.* *110*, 6877–6879. 10.1021/ja00228a043.
24. Turner, Z. (2015). Molecular pnictogen activation by rare earth and actinide complexes. *Inorganics* *3*, 597.
25. Evans, W.J., and Lee, D.S. (2005). Early developments in lanthanide-based dinitrogen reduction chemistry. *Can. J. Chem.* *83*, 375–384. 10.1139/v05-014.
26. Evans, W.J., Rego, D.B., and Ziller, J.W. (2006). Synthesis, structure, and ¹⁵N NMR studies of paramagnetic lanthanide complexes obtained by reduction of dinitrogen. *Inorg. Chem.* *45*, 10790–10798. 10.1021/ic061485g.
27. Evans, W.J., Lorenz, S.E., and Ziller, J.W. (2009). Investigating metal size effects in the Ln₂(μ-η²:η²-N₂) reduction system: Reductive reactivity with complexes of the largest and smallest trivalent lanthanide ions, La³⁺ and Lu³⁺. *Inorg. Chem.* *48*, 2001–2009. 10.1021/ic801853d.
28. Rinehart, J.D., Fang, M., Evans, W.J., and Long, J.R. (2011). A N₂³⁻ Radical-Bridged Terbium Complex Exhibiting Magnetic Hysteresis at 14 K. *J. Am. Chem. Soc.* *133*, 14236–14239. 10.1021/ja206286h.
29. MacDonald, M.R., Bates, J.E., Fieser, M.E., Ziller, J.W., Furche, F., and Evans, W.J. (2012). Expanding Rare-Earth Oxidation State Chemistry to Molecular Complexes of Holmium(II) and Erbium(II). *J. Am. Chem. Soc.* *134*, 8420–8423. 10.1021/ja303357w.
30. Woen, D.H., Chen, G.P., Ziller, J.W., Boyle, T.J., Furche, F., and Evans, W.J. (2017). End-On Bridging Dinitrogen Complex of Scandium. *J. Am. Chem. Soc.* *139*, 14861–14864. 10.1021/jacs.7b08456.
31. Ryan, A.J., Balasubramani, S.G., Ziller, J.W., Furche, F., and Evans, W.J. (2020). Formation of the end-on bound lanthanide dinitrogen complexes [(R₂N)₃Ln–N=N–Ln(NR₂)₃]²⁻ from divalent [(RN)₃Ln]¹⁻ salts (R = SiMe₃). *J. Am. Chem. Soc.* *142*, 9302–9313. 10.1021/jacs.0c01021.

32. Mondal, A., Price, C.G.T., Tang, J., and Layfield, R.A. (2023). Targeted Synthesis of End-On Dinitrogen-Bridged Lanthanide Metallocenes and Their Reactivity as Divalent Synthons. *Journal of the American Chemical Society* *145*, 20121-20131. 10.1021/jacs.3c07600.
33. Fang, M., Bates, J.E., Lorenz, S.E., Lee, D.S., Rego, D.B., Ziller, J.W., Furche, F., and Evans, W.J. (2011). $(N_2)_3^-$ Radical Chemistry via Trivalent Lanthanide Salt/Alkali Metal Reduction of Dinitrogen: New Syntheses and Examples of $(N_2)^{2-}$ and $(N_2)^{3-}$ Complexes and Density Functional Theory Comparisons of Closed Shell Sc^{3+} , Y^{3+} , and Lu^{3+} versus $4f^9 Dy^{3+}$. *Inorg. Chem.* *50*, 1459-1469. 10.1021/ic102016k.
34. Demir, S., Gonzalez, M.I., Darago, L.E., Evans, W.J., and Long, J.R. (2017). Giant coercivity and high magnetic blocking temperatures for N_2^{3-} radical-bridged dilanthanide complexes upon ligand dissociation. *Nat. Commun.* *8*, 2144. 10.1038/s41467-017-01553-w.
35. Lv, Z.-J., Huang, Z., Zhang, W.-X., and Xi, Z. (2019). Scandium-Promoted Direct Conversion of Dinitrogen into Hydrazine Derivatives via N–C Bond Formation. *J. Am. Chem. Soc.* *141*, 8773-8777. 10.1021/jacs.9b04293.
36. Fang, M., Lee, D.S., Ziller, J.W., Doedens, R.J., Bates, J.E., Furche, F., and Evans, W.J. (2011). Synthesis of the $(N_2)^{3-}$ Radical from Y^{2+} and Its Protonolysis Reactivity To Form $(N_2H_2)^{2-}$ via the $Y[N(SiMe_3)_2]_3/KC_8$ Reduction System. *J. Am. Chem. Soc.* *133*, 3784-3787. 10.1021/ja1116827.
37. Shephard, J.J., Berryman, V.E.J., Ochiai, T., Walter, O., Price, A.N., Warren, M.R., Arnold, P.L., Kaltsoyannis, N., and Parsons, S. (2022). Covalent bond shortening and distortion induced by pressurization of thorium, uranium, and neptunium tetrakis aryloxides. *Nature Commun.* *13*, 5923. 10.1038/s41467-022-33459-7.
38. Lateskey, S., Keddington, J., McMullen, A.K., Rothwell, I.P., and Huffman, J.C. (1985). Chemistry of sterically crowded aryloxide ligands. 5. Synthesis, structure, spectroscopic properties, and electrochemical behavior of group 4 metal derivatives containing bulky aryloxide ligands. *Inorg. Chem.* *24*, 995-1001. 10.1021/ic00201a007.
39. David, F.H. (2008). About low oxidation states, hydration and covalence properties of f elements. *rca - Radiochimica Acta* *96*, 135-144. doi:10.1524/ract.2008.1470.
40. Evans, W.J. (2016). Tutorial on the role of cyclopentadienyl ligands in the discovery of molecular complexes of the rare-earth and actinide metals in new oxidation states. *Organometallics* *35*, 3088-3100. 10.1021/acs.organomet.6b00466.
41. Bae, D.Y., Lee, G., and Lee, E. (2021). Fixation of Dinitrogen at an Asymmetric Binuclear Titanium Complex. *Inorg. Chem.* *60*, 12813-12822. 10.1021/acs.inorgchem.1c01050.
42. Komori, K., Oshita, H., Mizobe, Y., and Hidai, M. (1989). Preparation and properties of molybdenum and tungsten dinitrogen complexes. 25. Catalytic conversion of molecular nitrogen into silylamines using molybdenum and tungsten dinitrogen complexes. *J. Am. Chem. Soc.* *111*, 1939-1940. 10.1021/ja00187a092.
43. Duman, L.M., and Sita, L.R. (2017). Closing the Loop on Transition-Metal-Mediated Nitrogen Fixation: Chemoselective Production of $HN(SiMe_3)_2$ from N_2 , Me_3SiCl , and $X-OH$ ($X = R, R_3Si$, or Silica Gel). *J. Am. Chem. Soc.* *139*, 17241-17244. 10.1021/jacs.7b08859.
44. Falcone, M., Chatelain, L., Scopelliti, R., Živković, I., and Mazzanti, M. (2017). Nitrogen reduction and functionalization by a multimetallic uranium nitride complex. *Nature* *547*, 332. 10.1038/nature23279.
45. Suzuki, S., Ishida, Y., Kameo, H., Sakaki, S., and Kawaguchi, H. (2020). Counterion Dependence of Dinitrogen Activation and Functionalization by a Diniobium Hydride Anion. *Angew. Chem. Int. Ed.* *59*, 13444-13450. <https://doi.org/10.1002/anie.202006039>.
46. Grubel, K., Brennessel, W.W., Mercado, B.Q., and Holland, P.L. (2014). Alkali Metal Control over N–N Cleavage in Iron Complexes. *J. Am. Chem. Soc.* *136*, 16807-16816. 10.1021/ja507442b.

47. Kawaguchi, H., and Matsuo, T. (2004). Aryloxiide-based multidentate ligands for early transition metals and f-element metals. *J. Organomet. Chem.* *689*, 4228-4243. <https://doi.org/10.1016/j.jorganchem.2004.08.004>.
48. Marcus, Y. (1985). Thermodynamic functions of transfer of single ions from water to nonaqueous and mixed solvents: Part 3 - Standard potentials of selected electrodes. *Pure Appl. Chem.*, *57*, 1129-1132. <http://dx.doi.org/10.1351/pac198557081129>.
49. Manriquez, J.M., and Bercaw, J.E. (1974). Preparation of a dinitrogen complex of bis(pentamethylcyclopentadienyl)zirconium(II). Isolation and protonation leading to stoichiometric reduction of dinitrogen to hydrazine. *J. Am. Chem. Soc.* *96*, 6229-6230. 10.1021/ja00826a071.
50. Knobloch, D.J., Lobkovsky, E., and Chirik, P.J. (2010). Dinitrogen cleavage and functionalization by carbon monoxide promoted by a hafnium complex. *Nature Chem.* *2*, 30-35. 10.1038/nchem.477.
51. Kim, S., Loose, F., and Chirik, P.J. (2020). Beyond Ammonia: Nitrogen–Element Bond Forming Reactions with Coordinated Dinitrogen. *Chem. Rev.* *120*, 5637-5681. 10.1021/acs.chemrev.9b00705.
52. Hanna, T.E., Lobkovsky, E., and Chirik, P.J. (2009). Dinitrogen Complexes of Bis(cyclopentadienyl) Titanium Derivatives: Structural Diversity Arising from Substituent Manipulation. *Organometallics* *28*, 4079-4088. 10.1021/om900282u.
53. Lv, Z.-J., Wei, J., Zhang, W.-X., Chen, P., Deng, D., Shi, Z.-J., and Xi, Z. (2020). Direct transformation of dinitrogen: synthesis of N-containing organic compounds via N–C bond formation. *National Science Review* *7*, 1564-1583. 10.1093/nsr/nwaa142 %J National Science Review.
54. West, R., Ishikawa, M., and Bailey, R.B. (1966). Anionic Rearrangement of Hydrazines. II.1 Isomers of Bis(organosilyl)hydrazines2. *J. Am. Chem. Soc.* *88*, 4648-4652. 10.1021/ja00972a022.
55. Siedschlag, R.B., Bernales, V., Vogiatzis, K.D., Planas, N., Clouston, L.J., Bill, E., Gagliardi, L., and Lu, C.C. (2015). Catalytic silylation of dinitrogen with a dicobalt complex. *J. Am. Chem. Soc.* *137*, 4638-4641. 10.1021/jacs.5b01445.
56. Chalkley, M.J., Drover, M.W., and Peters, J.C. (2020). Catalytic N₂-to-NH₃ (or -N₂H₄) Conversion by Well-Defined Molecular Coordination Complexes. *Chem. Rev.* *120*, 5582-5636. 10.1021/acs.chemrev.9b00638.
57. Qing, G., Ghazfar, R., Jackowski, S.T., Habibzadeh, F., Ashtiani, M.M., Chen, C.-P., Smith, M.R., and Hamann, T.W. (2020). Recent Advances and Challenges of Electrocatalytic N₂ Reduction to Ammonia. *Chem. Rev.* *120*, 5437-5516. 10.1021/acs.chemrev.9b00659.
58. Garrido-Barros, P., Derosa, J., Chalkley, M.J., and Peters, J.C. (2022). Tandem electrocatalytic N₂ fixation via proton-coupled electron transfer. *Nature* *609*, 71-76. 10.1038/s41586-022-05011-6.